2014 5th IEEE RAS & EMBS International Conference on
Biomedical Robotics and Biomechatronics (BioRob)
August 12-15, 2014. São Paulo, Brazil

A Parallel Remote Center of Motion Mechanism for Needle-Based Medical Interventions

Mostafa Hadavand, Michael D. Naish, *Member, IEEE*, Rajni V. Patel, *Life Fellow, IEEE*

***Abstract*— A novel parallel Remote Center of Motion (RCM) mechanism is proposed for a surgical robot designed to perform minimally invasive needle-based interventions for lung cancer diagnosis and treatment. The proposed robot provides four degrees of freedom (DOFs) to orient and move a surgical needle within a spherical coordinate system. The RCM is beneath the skin surface to minimize the invasiveness of the surgical procedure while providing the required workspace. This compact, patient-mounted robot benefits from a design capable of measuring the pure interaction forces between the needle and the tissue. In this paper, the mechanism design and its specifications are described. The kinematic analysis is presented and isotropy of the mechanism for targeting tumors is studied. Finally, the performance of the proposed robot is evaluated experimentally.**

I. INTRODUCTION

Minimally invasive cancer diagnosis and treatment frequently involves needle-based interventions for image-guided biopsy, ablation, drug delivery and brachytherapy. The success rate of these interventions depends on the precise insertion of the needle into soft tissue organs such as the lung and liver [1]. While advanced imaging technologies such as Computed Tomography (CT) provide accurate localization of cancerous tumors, manual delivery of needle-based interventions often does not provide the accuracy required for the procedure. In this regard, special purpose surgical robots have been developed to perform image-guided percutaneous procedures. AcuBot from Johns Hopkins University is an early example of such a robotic system [2]. It consists of three main parts, including a one-DOF radiolucent needle driver known as PAKY (Percutaneous Access of the KidneY), a two-DOF RCM mechanism that tilts the needle around two axes, and a passive positioning arm attached to a 3-DOF X-Y-Z stage that mounts to the scanner bed [3]. In percutaneous procedures an RCM is not necessary because after passing through skin it is not possible to reorient the needle. However, an RCM would be useful if the needle was to be inserted through a trocar. Innomotion (Innomedic Inc., Herxheim, Germany), is another example of a robotic manipulator that is mounted on the scanner bed. It is used for prostate biopsy under Magnetic Resonance Imaging (MRI) guidance [4]. Being attached to the bed provides a stable platform for the robotic manipulator, but movements of the patient relative to the bed introduce errors in both image–robot registration and positioning of the needle [5]. The concept of mounting a robotic manipulator on the patient's body has been proposed to passively compensate for such motions [6], [7]. Robopsy from MIT is a patient-mounted robotic manipulator developed for lung biopsy [8]. This compact robot provides the DOFs required for percutaneous biopsy, including two tilt angles for needle orientation (pitch and yaw), selective gripping of the needle, and needle insertion/retraction. Robopsy utilizes a parallel spherical mechanism that improves its rigidity and has several actuators near the base of the robot. It provides an RCM; however, there is an 8 mm offset between the provided center of rotation and the patient's body.

The robot proposed in this paper is developed to support different types of needle-based interventions for minimally invasive cancer diagnosis and treatment. The mechanical design, along with the use of a trocar to introduce the needle into the body cavity, makes it possible to directly measure the interaction forces between the needle and the tissue. It has a novel parallel RCM mechanism with a simple analytical kinematic solution. The proposed mechanism provides four decoupled DOFs and has good manipulability and directional uniformity within the required workspace. The subcutaneous location of the RCM is the main advantage of the proposed robot over the exiting patient-mounted robotic systems. It helps to minimize the invasiveness of the surgical procedure while providing the required workspace. The design is compact and lightweight without compromising the structural stiffness of the system. Having the robot fixed to the patient's body reduces errors that may be caused by physiological motions such as respiration and repositioning of the patient during the surgical procedure. The rest of this paper is organized as follows: Section II defines the required specifications of the robot. Section III explains the details of the robot design. The kinematics of the mechanism are studied in Section IV. Finally, Section V presents the evaluation of the mechanism and Section VI concludes the paper.

The authors are with Canadian Surgical Technologies and Advanced Robotics (CSTAR), Lawson Health Research Institute, London, Canada. M. Hadavand is also with the Biomedical Engineering Graduate Program, Western University. M.D. Naish is also with the Department of Mechanical and Materials Engineering and the Department of Electrical and Computer Engineering, Western University. R.V. Patel is also with the Department of Electrical and Computer Engineering and the Department of Surgery, Western University (emails: mhadavan@uwo.ca, rvpatel@uwo.ca, mnaish@uwo.ca).

This research is supported by the Natural Sciences and Engineering Research Council (NSERC) of Canada under grants RGPIN-1345 (R.V. Patel), and 312383 (M.D. Naish); and by an NSERC-CIHR (Canadian Institutes for Health Research) Collaborative Health Research Projects Grant #398137-2011 (PI: R.V. Patel); and by infrastructure grants from the Canada Foundation for Innovation awarded to CSTAR and to Western University. Financial support for M. Hadavand has also been provided through an NSERC Collaborative Research and Training Experience (CREATE) program grant #371322-2009 in Computer-Assisted Medical Interventions (CAMI).

II. MECHANISM SPECIFICATIONS

The proposed design is based on consideration of the requirements for the minimally invasive delivery of needle-based interventions for lung cancer diagnosis and treatment. During such interventions, the surgical needle is introduced into the patient's body using a trocar, which is the main difference from percutaneous interventions. The most common types of needle-based interventions that involve the use of a trocar include image-guided needle biopsy, Radio Frequency (RF) ablation, microwave ablation and high dose rate brachytherapy. All of these interventions were investigated and the surgical procedures were carefully studied through observation and consultation with thoracic surgeons.

A. Required Degrees of Freedom

Based on our observations, four DOFs were identified to perform a needle-based intervention with a robotic manipulator: Two rotations (i.e., Pitch and Yaw) about the entry port into the patient's body to target the tumor prior to inserting the needle inside tissue, one translational motion to insert the needle towards the target after achieving the correct targeting angles, and the rotation of the needle around its longitudinal axis (i.e., Roll), which can be used to reduce static insertion displacement errors [9]. The entry port is determined based on the location of the tumor and a range of 30 degrees for the two targeting motions (Pitch and Yaw) was determined to be sufficient.

B. Remote Center of Motion

During a minimally invasive intervention, the surgical tool may be introduced into the patient's body through a trocar. In this way, it is possible to correct the needle's orientation prior to insertion into the target tissue, while during a percutaneous procedure no orientation correction is possible after passing through the skin. Thus, having a proper Remote Center of Motion mechanism is necessary to prevent damage to the patient's body by orienting the needle about a fixed point. Patient-mounted RCM mechanisms suffer from improper positioning of the RCM [8] due to the fact that it is not possible to shift the RCM downward to the proper position by moving the robot downward. However, the ideal position of the RCM is centered in the wall cavity through which the surgery is performed to minimize the damage. In the thoracic cavity, the ideal position of the RCM is between two adjacent ribs. If there is an offset between the location of the RCM and the ribs, the available workspace for orienting the surgical needle while it is inside the thoracic cavity would be limited by the ribs. Furthermore, the application of excessive forces to the ribs may result in a lot of pain for the patient after surgery. The proposed design is capable of moving the RCM downward up to a certain limit to maintain the compactness of the design. The RCM is moved 2 cm below skin level to maintain the required workspace while minimizing the forces applied to the adjoining ribs during the procedure.

C. Patient-Mounted, Modular Design

Fixing the robot into the patient's anatomy is a simple and effective approach to reduce the errors caused by the patient's motion relative to the bed. The proposed robot weighs about 1.6 kg and its overall size is 30×30×25 cm. Although, the robot is compact and lightweight, gaining better structural stiffness was the first priority. Thus, the RCM mechanism has a parallel structure that improves the robot's stiffness and in turn its targeting accuracy. Additionally, the robot benefits from a modular design to support different sizes of surgical needles.

D. Parallel RCM Mechanism

Double parallelogram mechanisms have been widely used in medical robotics to provide the RCM at the entry port into the patient's body [10], [11]. A fixed RCM, a wide range of motion, high manipulability and a simple analytical solution for the kinematics are the main features of a double parallelogram-based RCM. However, having a large number of linkages is the main drawback associated with this design. The proposed parallel RCM mechanism has two main kinematic chains (i.e., legs) that connect the body of the mechanism to the stationary base of the mechanism. The main leg of the mechanism provides the RCM in a way similar to the double parallelogram mechanism while having a fewer number of rigid linkages. As depicted in Fig. 1, the main leg has four linkages shown as colored bars and two motion constraints. The motion constraints (i.e., timing belts and pulleys) transfer rotation from Link 1 to Link 3 and from Link 2 to Link 4 to provide the RCM. The ancillary leg is connected to the main leg as depicted in Fig. 1, and forms the parallel configuration.

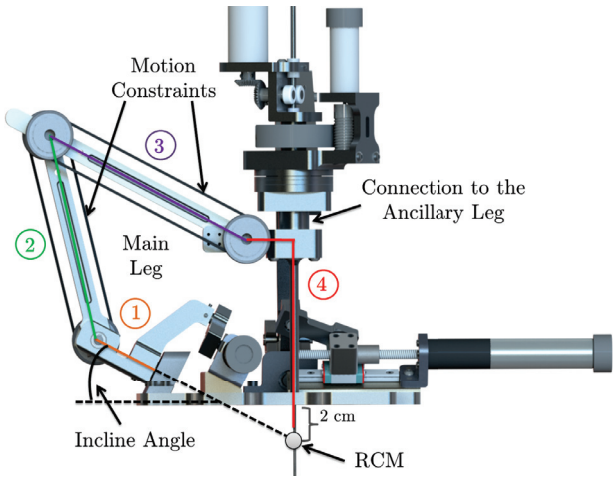

Fig. 1. The main leg of the parallel mechanism.

The RCM was moved below the skin surface while maximizing the available workspace by inclining each of the mechanism's legs downward as shown in Fig. 1 and placing the base of each leg at the appropriate position. There is a geometric relationship between the incline angle, the relative position of each leg and the length of Link 2. To move

the RCM downward, it is required to increase the length of Link 2 while increasing the incline angle. Since the proposed mechanism is intended to be mounted on the patient's body and needs to be compact, the amount that the RCM can be moved downward is limited.

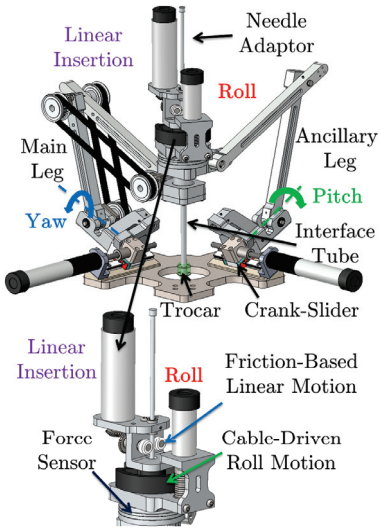

Fig. 2. Details of the mechanism and its degrees of freedom.

Fig. 2 introduces the robot DOFs and provides the details on the actuation methods. Pitch and Yaw are used to tilt the needle around the RCM to target the tumors based on medical image guidance. These two DOFs are actuated using crank–slider mechanisms driven by linear actuators (i.e., spindle and ball-screw). The combination of the crank–slider and ball screw provides a considerable mechanical advantage to provide the torque required to tilt the trocar, while minimizing the amount of angular backlash in the Pitch and Yaw DOFs. As can be seen in Fig. 2, the Pitch and Yaw DOFs rotate the interface tube to perform the targeting tasks while Roll and Linear insertion are actuated independently using two actuators located at the top of the mechanism. The interface tube goes inside the trocar so the robot can orient the trocar without any interaction between the needle and trocar. The needle-adaptor contains the needle and is actuated by the Roll and Linear insertion motors to move through a hollow force sensor (Nano43 6 DOF force/torque sensor, ATI Industrial Automation), the body of the mechanism, the interface tube and the trocar. The force sensor is attached to the mechanism's legs from one side while the other side supports the Roll and Linear insertion actuation system. As a result, the needle has no interaction with the trocar and directly interacts with the tissue.

E. Modular Design to Support Different Needle Sizes

Based on our investigations and consultations with radiologists and thoracic surgeons, it was concluded that needle sizes between 25 GA to 13 GA are typically used for lung cancer diagnosis and treatment. A simple approach was chosen to handle different needle sizes. A tubular needle adaptor (shown in Fig. 3) is designed for each needle size,

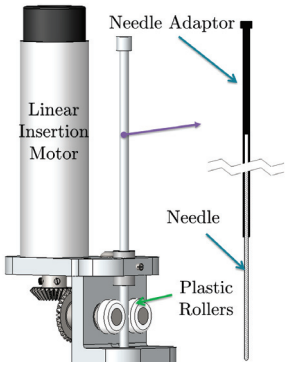

Fig. 3. Needle Adaptor and Linear Insertion Actuation.

with a fixed outside diameter and a hole in the middle sized for the corresponding needle. Thus, each needle size has its own simple adaptor, and all of the adaptors have the same outside diameter. The adaptors are squeezed between two plastic rollers to provide friction-based linear motion.

III. KINEMATIC ANALYSIS

Finding an analytical solution for parallel mechanisms is often difficult due to the intrinsic complexity of such mechanisms.

A. Forward Kinematics

There are two kinematic chains (i.e., legs) that connect the robot's end effector to its base. In order to find the forward kinematics of the robot, only one of the legs is considered to derive the forward kinematics equation. Fig. 4 shows the joint variables and the coordinate systems attached to the right leg of the robot. The coordinate systems are chosen based on the Denavit-Hartenburg (DH) convention for affixing frames to links, as presented in [12].

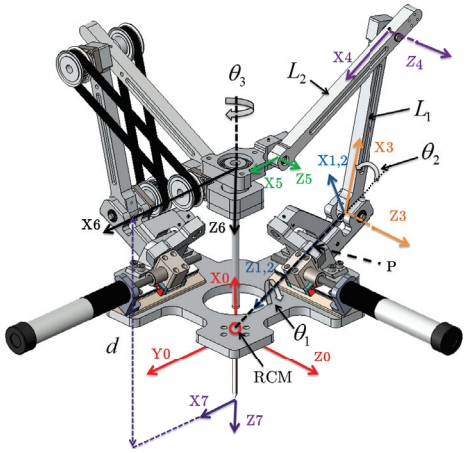

Fig. 4. Coordinate frames attached to the right leg of the robot.

Using the coordinate systems and joint variables introduced in Fig. 4, the DH parameters are as shown in Table I. The parameters θ_1, θ_2, θ_3 and d represent the Pitch, Yaw, Roll and linear insertion motions respectively. L_1 and L_2 are the lengths of the linkages and P is the distance between

centers of the base coordinate system (Frame 0), which is located at the RCM, and Frame 1. The angle ϕ provides an offset distance of $L_1\sin(\phi)$ between the centers of Frame 5 (last joint of the leg) and Frame 6 (surgical tool axis). See [13] for a detailed explanation of angle ϕ and the offset it provides.

TABLE I
DENAVIT-HARTENBERG PARAMETERS

i	θ_i	d_i	a_i	α_{i-1}
1	α	P	0	$-\pi/2$
2	θ_1	0	0	0
3	$\theta_2-\pi/2$	0	0	$\pi/2$
4	$\pi-\theta_2$	0	L_1 (130 mm)	0
5	$\theta_2+\phi-\pi/2$	0	L_2 (120 mm)	0
6	θ_3	0	$L_1\sin(\phi)$	0
7	d	0	0	0

The transformation matrix, ${}^0_7T$, between Frames 0 and 7 (tip of the needle) represents the forward kinematics of the right leg as a function of joint variables θ_1, θ_2, θ_3 and d. The same approach can be used for the left leg of the robot to derive the forward kinematics. The forward kinematics for both legs yield the same results since they share the same end effector and base coordinate frames. There are two sets of joint variables that can provide the forward kinematics of the robot, namely: θ_1, θ_2, θ_3, d and $\acute{\theta}_1$, $\acute{\theta}_2$, $\acute{\theta}_3$, $\acute{d}$, corresponding to each leg of the mechanism. However, the joint variables that are actuated and in turn measured must be used to derive the forward kinematics. Considering the right leg of the robot, it can be realized that joint variables θ_3 and d are actuated by the Roll and linear insertion motors, respectively, and θ_1 is actuated using a crank-slider mechanism (see Fig. 2), while θ_2 is not directly actuated. There is the same situation for the other leg of the robot. The parallel configuration makes it possible to actuate Pitch and Yaw (i.e., θ_1, $\acute{\theta}_1$) at the base of the robot to reduce the floating inertia. These two DOFs tilt the needle/probe around the RCM to target the needle. In this regard, it is required to find θ_2 as a function of θ_1 and $\acute{\theta}_1$ and then the forward kinematics is based on the desired four joint variables that are actuated (i.e., θ_1, $\acute{\theta}_1$, θ_3, d). Considering geometry-based relations between frames attached to the legs, θ_2 can be found as:

$$\theta_2=\alpha-\arctan\left(\frac{U}{V}\right)+\frac{\pi}{2}-\phi, \tag{1}$$

where U and V are functions of θ_1 and $\acute{\theta}_1$. The combination of ${}^0_7T$ and (1) provides the analytical forward kinematics of the proposed parallel mechanism using the actuated joint variables. Table II presents the specified range of motion at each degree of freedom.

B. Inverse Kinematics

Given the desired position of the robot's end effector in the base coordinate system, $[XYZ]^T$, the inverse kinematics is derived as shown in (2):

TABLE II
RANGE OF MOTION AT EACH DEGREE OF FREEDOM

DOF	Range of Motion
Pitch (θ_1)	$\pm22.5^\circ$
Yaw ($\acute{\theta}_1$)	$\pm22.5^\circ$
Insertion (d)	20 cm below the RCM
Roll (θ_3)	0°–180°

$$\begin{aligned}
d&=\sqrt{X^2+Y^2+Z^2}+L_1\cos(\phi)\\
\theta_1&=\arctan(\mathbf{V}(3),\mathbf{V}(2)\sin(\alpha)-\mathbf{V}(1)\cos(\alpha))\\
\acute{\theta}_1&=\arctan(-\mathbf{V}(2),\mathbf{V}(3)\sin(\alpha)-\mathbf{V}(1)\cos(\alpha))
\end{aligned}\tag{2}$$

$$\text{where } \mathbf{V}=\begin{bmatrix}\dfrac{X}{\sqrt{X^2+Y^2+Z^2}}\\[2ex]\dfrac{Y}{\sqrt{X^2+Y^2+Z^2}}\\[2ex]\dfrac{Z}{\sqrt{X^2+Y^2+Z^2}}\end{bmatrix}.$$

C. Jacobian and Kinematic Performance

For each leg of the robot, a Jacobian matrix (J) can be derived that provides a linear transformation from joint velocities ($\dot{\Theta}$) to the Cartesian velocities of the end effector (v) expressed in any frame, as shown in (3) and (4):

$$\begin{aligned}
{}^7v_7&={}^7J(\Theta)\cdot\dot{\Theta}=\begin{bmatrix}j_{11}&j_{12}&0\\j_{21}&j_{22}&0\\0&0&1\end{bmatrix}\cdot\begin{bmatrix}\dot{\theta}_1\\\dot{\theta}_2\\\dot{d}\end{bmatrix}\\
\det({}^7J(\Theta))&=-\sin(\theta_2+\phi)(d-L_1\cos(\phi))^2
\end{aligned}\tag{3}$$

$$\begin{aligned}
{}^7w_7&={}^7J_w(\Theta)\cdot\dot{\Theta}=\begin{bmatrix}j_{w11}&j_{w12}&0\\j_{w21}&j_{w22}&0\\j_{w31}&0&1\end{bmatrix}\cdot\begin{bmatrix}\dot{\theta}_1\\\dot{\theta}_2\\\dot{\theta}_3\end{bmatrix}\\
\det({}^7J_w(\Theta))&=-\sin(\theta_2+\phi)
\end{aligned}\tag{4}$$

${}^7v_7$ and ${}^7w_7$ represent the absolute translational and rotational velocities of the end effector (i.e., needle's tip) expressed in the end-effector frame for the right leg. The same Jacobians can be found for the left leg. None of the Jacobians' singularities lie inside the workspace (as defined in Table II).

The Jacobian matrix can be used to analyse a mechanism's kinematic performance. Several measurements have been suggested to quantify the kinematic performance including the mechanism's isotropy [14]. However, for the proposed parallel mechanism, which is a combination of the two legs, there is not a linear mapping between the actuated DOFs (i.e., θ_1, $\acute{\theta}_1$, θ_3, d) and the end effector's velocities in Cartesian space, so a Jacobian matrix cannot be developed. In order to address this issue, the forward kinematics of the robot can be used to check the performance of the whole parallel mechanism. In this regard, at each point within

the robot's workspace, the joint variables can be changed by some small value to study the overall effect on the position of the end effector within Cartesian space. Pitch, Yaw and linear insertion (i.e., θ_1, $\acute{\theta}_1$ and d) are the three DOFs that determine the position of the end effector within Cartesian space. The Pitch and Yaw are the two important DOFs for targeting tumors, while the linear insertion is done independently after targeting is finalized and Pitch and Yaw are locked. Thus, uniformity in the Pitch and Yaw DOFs is of primary importance for the proposed parallel mechanism and needs to be studied. The Pitch and Yaw degrees of freedom correspond to end-effector motions along the Z and Y axes of the base frame as shown in Fig. 4. Thus, at each point within the robot's workspace, the joint variables corresponding to the Pitch and Yaw motions (θ_1, $\acute{\theta}_1$) may be changed by the same small value (i.e., $\theta_1 \pm \sigma$, $\acute{\theta}_1 \pm \sigma$) and the corresponding movements along Z and Y direction may be compared to find the ratio between them. Fig. 5 depicts the ratio variation within the workspace.

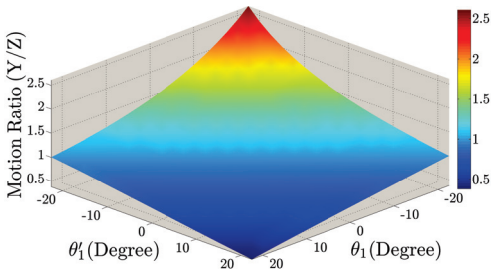

Fig. 5. Directional uniformity within the robot's workspace.

As shown in Fig. 5, the motion ratio varies between 0.4 and 2.6. The best condition at any insertion depth within the workspace occurs at the center of the workspace ($\theta_1 = 0$, $\acute{\theta}_1 = 0$), where the ratio is 1, which means a completely isotropic condition. It can also be realized that around the center of the workspace, the Pitch and Yaw degrees of freedom are completely decoupled.

IV. Experimental Evaluations of the Prototype

In order to effectively evaluate the robot's performance and assess its capabilities a series of experiments was conducted.

A. Workspace Evaluation

The proposed robot is capable of supporting a larger workspace as it provides a total range of 45° (±22.5°) for the two targeting degrees of freedom (i.e., the Pitch and Yaw).

The Insertion motion is actuated using two plastic rollers as was explained previously. Thus, the range of motion for the Insertion of the needle is not limited and only depends on the length of the needle adaptor. On the other hand, the roll motion has a range of motion of more than 180° which satisfies the requirements for the targeted applications.

B. RCM Assessment

In order to assess the RCM of the robot, the tip of the needle was placed at the RCM, while the needle was moved within the range of its workspace by applying sinusoidal motions to the Pitch and Yaw DOFs and its motion was tracked by an optical tracking system (Claron Technology Inc.), Fig. 6. The standard deviations of the RCM position along the X, Y and Z axes of the camera are 0.17 mm, 0.31 mm and 0.19 mm respectively. Thus, the mechanism is capable of providing a proper fixed centre of rotation for the surgical needle while it is inserted into the patient's body.

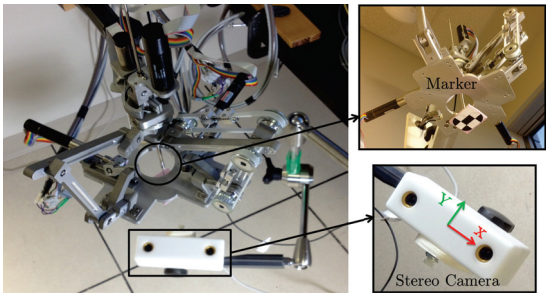

Fig. 6. Tracking the tip of the needle using an optical tracking system.

C. Path Planning

Tracking a predefined path with the tip of the needle was performed to evaluate the targeting capabilities of the robot. A circular path with a diameter of 20 mm was generated 100 mm beneath the RCM, parallel to the YZ plane of the base coordinate frame. Again, the tip of the needle was tracked by the stereo camera to assess the accuracy of the robot in tracking the desired path. Fig. 7 shows the desired and generated circular path. The maximum deviation from the desired circular path is 1 mm.

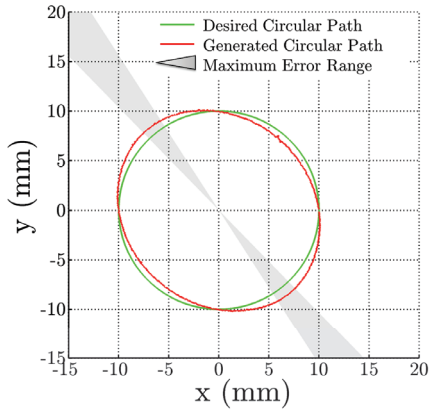

Fig. 7. The generated circular path and desired one in robot's base coordinate frame.

The path generation was performed using the analytical model of the robot and considering the calibrated lengths of the linkages. In other words, it was an open-loop position control without any feedback from the actual position of the end effector (i.e., tip of the needle). Thus, the tracking accuracy is affected by calibration error (accounting for kinematics and mechanical errors), and optical tracking error.

D. Force Measurements

Fig. 8 shows an experimental setup developed to measure the interaction forces between a surgical needle and an animal tissue sample (chicken breast). As can be seen in Fig. 8, the robot is attached to a human thoracic cavity model and the surgical needle is inserted into the cavity through a small trocar (standard 5 mm trcar). The needle was inserted 5 cm into the tissue and then retracted at a speed of 14 mm/sec. Fig. 9 shows the insertion force applied to the needle during the experiment, as recorded by the force sensor.

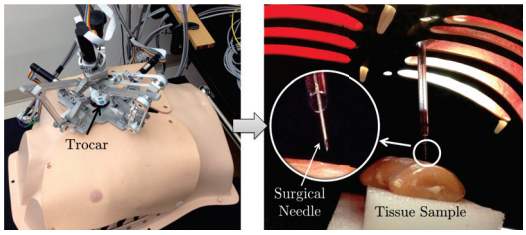

Fig. 8. Needle insertion into animal tissue using the proposed patient-mounted robot.

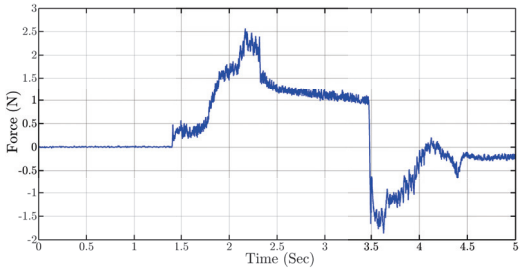

Fig. 9. Insertion force applied to the surgical needle.

V. CONCLUSIONS

A novel parallel RCM mechanism has been introduced for lung cancer diagnosis and treatment. It supports different types of needle-based interventions including biopsy, ablation and high-dose-rate brachytherapy. The proposed design is based on consideration of the challenges associated with patient-mounted robots and aims to address some of these by carefully considering the mechanical design. The RCM was moved downward to maintain the required workspace while minimizing the forces acting on the patient's body. The parallel design improves structural stiffness and also places actuators on the stationary base of the robot to decrease the floating inertia. There is a simple analytical solution for the kinematics of the proposed parallel mechanism and it has been shown that the end effector motion is well-conditioned within the required workspace. Although the proposed robot is lightweight, its weight is intended to be passively supported by a holder mechanism that uses constant-force springs while it is fixed to the patient's anatomy. Thus, physiological motions, and repositioning do not cause errors in positioning and registration. The prototype of the proposed robot has been evaluated through a series of experiments. Although the open-loop control of the robot provides the required targeting accuracy for the intended applications, further improvements are expected by integrating image guidance and using a master–slave control method. In this regard, the interventionist can control the orientation and position of the surgical needle remotely based on medical images (i.e., intra-operative ultrasound or CT).

REFERENCES

[1] N. Abolhassani, R. Patel, and M. Moallem, "Needle insertion into soft tissue: a survey," in *Medical Engineering and Physics*, vol. 29, pp. 413–431, 2007.

[2] D. Stoianovici, L. Whitcomb, J. Anderson, R. Taylor, and L. Kavoussi, "A modular surgical robotic system for image guided percutaneous procedures," in *Medical Image Computing and Computer-Assisted Interventions*. vol. 1496, pp. 404–410, 1998.

[3] D. Stoianovici, K. Cleary, A. Patriciu, D. Mazilu, A. Stanimir, N. Craciunoiu, V. Watson, and L. Kavoussi, "AcuBot: a robot for radiological interventions," *IEEE Transactions on Robotics and Automation*, vol. 19, pp. 927–930, 2003.

[4] A. Melzer, B. Gutmann, T. Remmele, R. Wolf, A. Lukoscheck, M. Bock, H. Bardenheuer, and H. Fischer, "INNOMOTION for percutaneous image-guided interventions," *IEEE Engineering in Medicine and Biology Magazine*, vol. 27, pp. 66–73, 2008.

[5] P. Berkelman, J. Troccaz, and P. Cinquin, "Body-supported medical robots: a survey," *Journal of Robotics and Mechatronics*, vol. 16, pp. 513–519, 2004.

[6] B. Maurin, B. Bayle, O. Piccin, J. Gangloff, M. de Mathelin, C. Doignon, P. Zanne, and A. Gangi, "A patient-mounted robotic platform for CT-scan guided procedures," *IEEE Transactions on Biomedical Engineering*, vol. 55, pp. 2417–2425, 2008.

[7] A. Seitel, C. J. Walsh, N. C. Hanumara, J. O. Shepard, A. H. Slocum, H. P. Meinzer, R. Gupta, and L. Maier-Hein, "Development and evaluation of a new image-based user interface for robot-assisted needle placements with the robopsy system," *Proceedings of the SPIE Medical Imaging Conference*, vol. 7261, Orlando, FL, Feb. 7–12, 2009, pp. 72610X-1–72610X-9.

[8] C. J. Walsh, Hanumara, N. C., Slocum, A. H., Shepard, "A patient-mounted, telerobotic tool for CT-guided percutaneous interventions," *Journal of Medical Devices*, vol. 2, no. 1, pp. 011007, 2008.

[9] S. Badaan, D. Petrisor, C. Kim, P. Mozer, D. Mazilu, L. Gruionu, A. Patriciu, K. Cleary, and D. Stoianovici, "Does needle rotation improve lesion targeting?," *The International Journal of Medical Robotics and Computer Assisted Surgery*, vol. 7, pp. 138–147, 2011.

[10] J. Rosen, J. D. Brown, L. Chang, M. Barreca, M. Sinanan, and B. Hannaford, "The BlueDRAGON—a system for measuring the kinematics and dynamics of minimally invasive surgical tools in-vivo," in *IEEE International Conference on Robotics and Automation*, Washington, DC, May 11–15, 2002, pp. 1876–1881.

[11] M. Hadavand, A. Mirbagheri, S. Behzadipour, and F. Farahmand, "A novel remote center of motion mechanism for the force-reflective master robot of haptic tele-surgery systems," *The International Journal of Medical Robotics and Computer Assisted Surgery*, 2013.

[12] J. J. Craig, Introduction to Robotics: Mechanics and Control, Prentice Hall: Englewood Cliffs, NJ, 2005.

[13] A. Faraz and S. Payandeh, "A robotic case study: optimal design for laparoscopic positioning stands," *The International Journal of Robotics Research*, vol. 17, pp. 986–995, September 1998.

[14] J. K. Salisbury and J. J. Craig, "Articulated hands: force control and kinematic issues," *The International Journal of Robotics Research*, vol. 1, pp. 4–17, 1982.

[15] G. Picod, A. C. Jambon, D. Vinatier, and P. Dubois, "What can the operator actually feel when performing a laparoscopy?," *Surgical Endoscopy And Other Interventional Techniques*, vol. 19, pp. 95–100, 2005.